Spin dynamics in the skyrmion-host lacunar spinel GaV_4S_8

G. Pokharel,[1,2,3,*] H. Suriya Arachchige,[1,2] S. Gao,[2,4] S.-H. Do,[2] R. S. Fishman,[2] G. Ehlers,[5] Y. Qiu,[6] J. A. Rodriguez-Rivera,[6] M. B. Stone,[4] H. Zhang,[1] S. D. Wilson,[3] D. Mandrus,[7,2,1] and A. D. Christianson[2,†]

[1]*Department of Physics & Astronomy, University of Tennessee, Knoxville, Tennessee 37996, USA*
[2]*Materials Science & Technology Division, Oak Ridge National Laboratory, Oak Ridge, Tennessee 37831, USA*
[3]*Materials Department and California Nanosystems Institute, University of California Santa Barbara, Santa Barbara, California 93106, USA*
[4]*Neutron Scattering Division, Oak Ridge National Laboratory, Oak Ridge, Tennessee 37831, USA*
[5]*Neutron Technologies Division, Oak Ridge National Laboratory, Oak Ridge, Tennessee 37831, USA*
[6]*NIST Center for Neutron Research, National Institute of Standards and Technology, Gaithersburg, Maryland 20899, USA*
[7]*Department of Materials Science & Engineering, University of Tennessee, Knoxville, Tennessee 37996, USA*

(Received 23 October 2021; accepted 9 December 2021; published 20 December 2021)

In the lacunar spinel GaV_4S_8, the interplay of spin, charge, and orbital degrees of freedom produces a rich phase diagram that includes an unusual Néel-type skyrmion phase composed of molecular spins. To provide insight into the interactions underlying this complex phase diagram, we study the spin excitations in GaV_4S_8 through inelastic neutron scattering measurements on polycrystalline and single crystal samples. Using linear spin wave theory, we describe the spin wave excitations using a model where V_4 clusters decorate an fcc lattice. The effective cluster model includes a ferromagnetic interaction and a weaker antisymmetric Dzyaloshinskii-Moriya interaction between the neighboring molecular spins. Our work clarifies the spin interactions in GaV_4S_8 and supports the picture of interacting molecular clusters.

DOI: 10.1103/PhysRevB.104.224425

I. INTRODUCTION

Magnetic skyrmions are topological spin textures characterized by an integer topological number and have potential for applications in spintronics devices [1–5]. Since the first discovery of the Bloch-type skyrmions in MnSi [6], different types of magnetic skyrmions have been identified [7–9]. Among them, the Néel-type skrymion first realized in the polar system GaV_4S_8 has drawn great attention [10–15]. Distinct from the spin whorls in the Bloch-type skyrmions, Néel-type skyrmions are composed of spins rotating in the radial planes, which provides new opportunities for skyrmion manipulations [16–18].

GaV_4S_8 belongs to the lacunar spinel family of compounds with a chemical formula AM_4X_8 (A = Ga, Ge; M = V, Mo, Nb, and Ta; X = S and Se) [20–31], where the magnetic M ions form a breathing pyrochlore lattice as shown in Fig. 1(a). GaV_4S_8 is a magnetic semiconductor where the magnetism is associated with the unpaired valence electrons localized in the V_4 tetrahedra [32]. Assuming Ga and S take their most common valence configuration, charge balance yields $Ga^{3+}V_4^{3.25+}S_8^{2-}$ with seven valence electrons per V_4 cluster. Due to the short V-V metal bonds in the smaller V_4 tetrahedra, the V $3d$ bands hybridize with each other, leading to a molecular spin-1/2 that is almost evenly distributed across the V_4 tetrahedra [33]. At temperatures below $T_s \sim 44$ K, GaV_4S_8 undergoes a cubic ($F\bar{4}3m$)-rhombohedral ($R3m$) transition due to a Jahn-Teller (JT) distortion, which elongates the V_4 tetrahedra along the {111} directions and results in an easy axis anisotropy for the V_4 spins as shown in Fig. 1. This anisotropy stabilizes a ferromagnetic (FM) ground state below $T_c = 6$ K [10,11,14]. For temperatures between T_c and the long range order transition of $T_N = 12.8$ K, GaV_4S_8 has a thermal-fluctuation-stabilized cycloidal phase with a periodicity of ∼20 nm. The Néel-type skyrmion phase emerges from the cycloidal phase in an applied magnetic field [10,11,14].

Although the competition between the ferromagnetic exchange interactions and the Dzyaloshinskii-Moriya (DM) interaction has been proposed to induce the spin winding in GaV_4S_8, the interactions between the V_4 spins are still not determined experimentally. Here we report an inelastic neutron scattering (INS) study of the spin excitations in GaV_4S_8 and determine the coupling strengths between the V_4 spins. The powder averaged INS spectra reveal spin wave excitations with a bandwidth of ∼6 meV, and the wave vector dependence of the scattering intensity is strongly modulated by the V_4 structure factor. For the crystal sample, dispersive spin wave excitations are observed along the high symmetry directions, and the spectra are reproduced using a classical Heisenberg model that incorporates the ferromagnetic exchange interactions and the DM interactions.

II. EXPERIMENTAL DETAILS

Polycrystalline samples of GaV_4S_8 were synthesized by solid state reaction. Stoichiometric amounts of Ga (99.999%), V (99.5%), and S (99.9995%), purchased from Alfa Aesar, were ground together inside a glove box and then pressed

*ganeshpokharel@ucsb.edu
†christiansad@ornl.gov

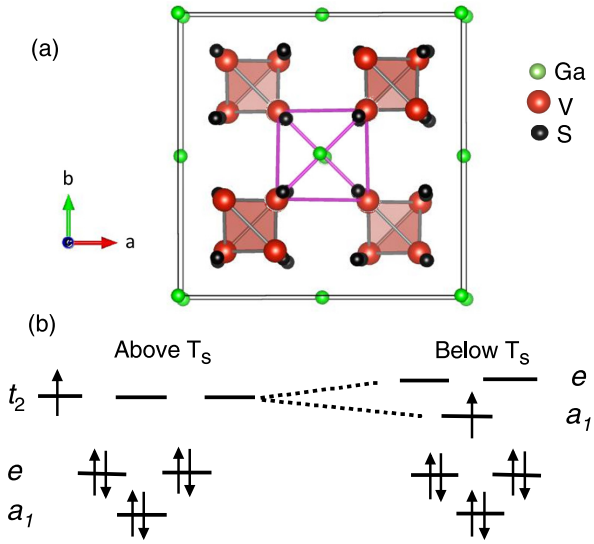

FIG. 1. (a) Crystal structure of GaV_4S_8 highlighting the breathing pyrochlore V sublattice composed of a periodic arrangement of large and small V_4 tetrahedra. (b) Molecular orbital diagrams of the V_4 tetrahedra in GaV_4S_8 with (below T_s) and without (above T_s) the Jahn-Teller distortion [19].

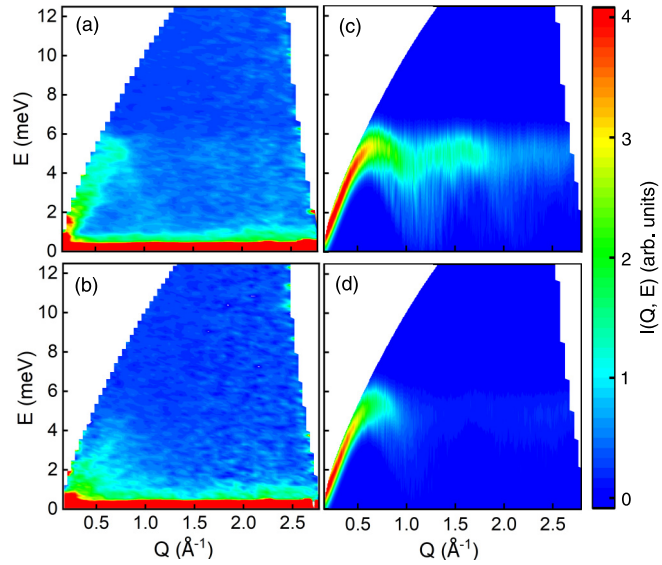

FIG. 2. Powder-averaged INS spectra of GaV_4S_8 measured on SEQUOIA with $E_i = 18$ meV at (a) 5 K in the FM ordered magnetic phase and (b) 20 K in the paramagnetic phase. Panels (c) and (d) show the calculated powder-averaged spin excitation spectra in the magnetically ordered state of GaV_4S_8. The form factor of a single V^{3+} ion is taken into account in (c), whereas the form factor of V_4 tetrahedra is taken into account in (d) demonstrating the importance of the molecular nature of the V_4 tetrahedra.

into a 0.5-in.-diameter pellet. The pellet was slowly heated to 800 °C over a period of 24 h and the phase purity was checked by Cu *K*-alpha x-ray diffraction (XRD). The heating process was repeated until the XRD patterns indicated the presence of a single phase.

GaV_4S_8 crystals were grown by the chemical vapor transport (CVT) technique with iodine as the transport agent. Approximately 5 wt % of iodine was mixed with a 2.5-g polycrystalline sample of GaV_4S_8 and then sealed in a quartz tube. The tube was placed inside a two-zone furnace and a temperature gradient of approximately 50 °C was maintained. The temperatures of the hot end and cold end of the quartz tube were regulated to 850 °C and 800 °C respectively. The growth period was about eight weeks. The mass of crystals grown with this protocol and used in the neutron scattering measurements was ∼100 mg.

The INS measurements of polycrystalline samples were performed on the Fine-Resolution Fermi Chopper Spectrometer SEQUOIA [34] at the Spallation Neutron Source (SNS) at Oak Ridge National Laboratory (ORNL) with incident energies, E_is of 18 and 40 meV. The sample consisted of a finely ground polycrystalline sample with a mass of 5 g packed inside an aluminum cylinder ($\phi = 9$ mm) and mounted on a closed-cycle refrigerator (CCR). The measurements were performed in the high resolution mode with the Fermi chopper set to 300 and 240 Hz for $E_i = 40$ and 18 meV, respectively. No magnetic scattering above 7 meV was discernible in the $E_i = 40$-meV data and hence the corresponding data are not shown here. To remove the background contribution, the scattering from an empty sample holder has been subtracted from the data presented in Fig. 2.

The INS measurements of single crystals were performed using the Multi-Axis Chopper Spectrometer MACS [35] at the NIST center for neutron research (NCNR). Thirteen crystals with a total mass of ∼1.2 g were coaligned with the (*HHL*) plane horizontal. For the MACS experiments, a helium flow cryostat with a base temperature of 1.7 K was employed. A Be filter was placed between the sample and analyzer. To cover a large range of momentum transfer, the sample was rotated about the vertical axis over a range of 120° in 2° steps. The measurements were performed with a fixed final energy E_f of 5 meV. A measurement of an empty sample holder was collected with the same configuration for background subtraction. All single crystal INS measurements shown have had this background subtraction applied unless otherwise noted.

III. RESULTS AND DISCUSSION

Figure 2 presents the powder-averaged INS spectra of GaV_4S_8 measured using SEQUOIA with $E_i = 18$ meV at $T = 5$ and 20 K. In the FM phase at 5 K, the spectra exhibit a single excitation emerging from $Q = 0$ with a bandwidth of ∼6 meV. At larger wave-vector transfers the scattering decreases in intensity consistent with the cross section being magnetic in origin. With a higher incident neutron energy of $E_i = 40$ meV (not shown), we confirm that no additional magnetic scattering is observed beyond that evident in Fig. 2(a). At 20 K [Fig. 2(b)], weak diffuse inelastic scattering is observed. This indicates that the spin-spin correlations survive above $T_N = 12.8$ K as expected for a material with geometrical frustration such as GaV_4S_8.

The INS data collected on the single crystal array at $T = 1.7$ K in the FM phase are summarized in Fig. 3. Reciprocal lattice unit (r.l.u.) indices are denoted in the cubic space group for convenience. Spin waves emanating from the ferromagnetic wave vectors are observed along the (001) and (110)

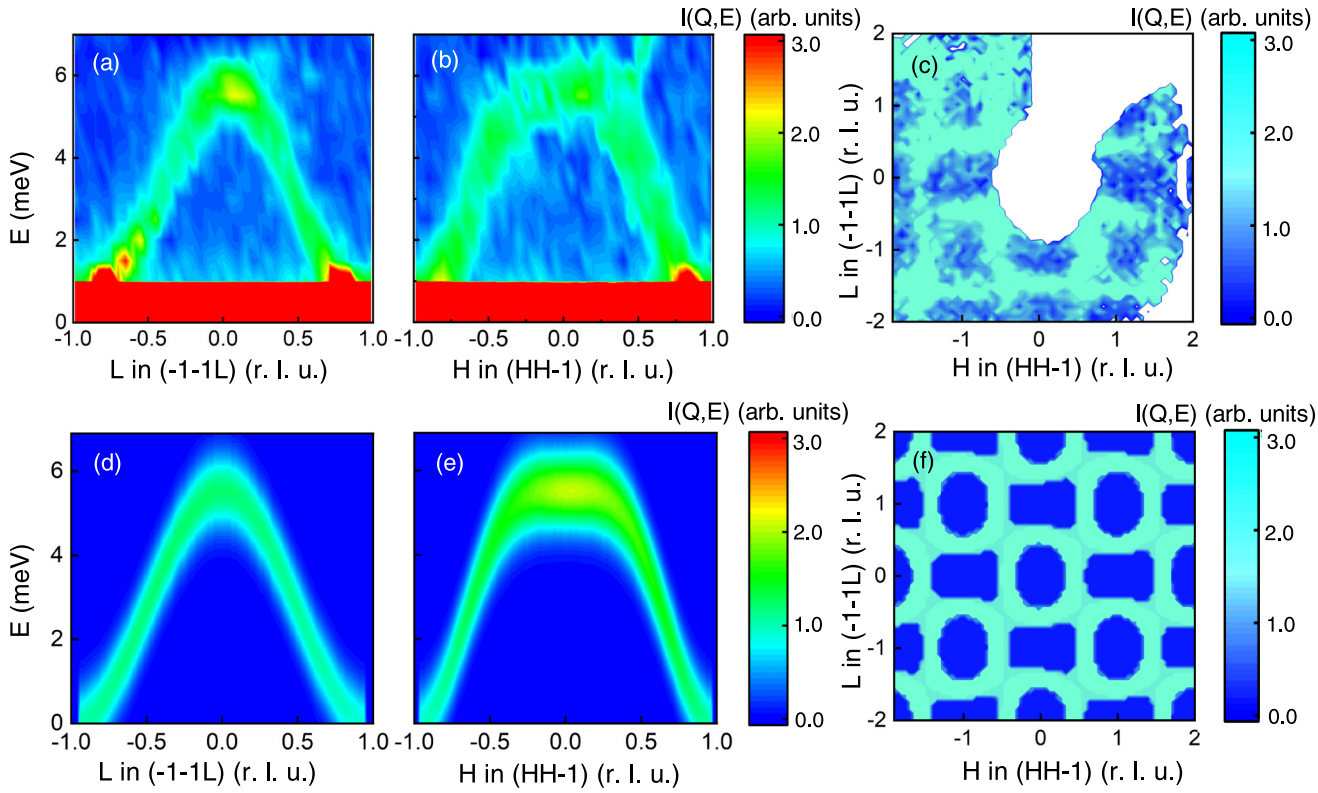

FIG. 3. Inelastic neutron scattering intensity as a function of energy and wave-vector transfer for GaV_4S_8 at T=1.7 K. Spin wave excitations along the (a) $(-1-1L)$ and (b) $(HH-1)$ directions at $T = 1.7$ K measured using the MACS instrument. (c) Constant-energy slice of the INS spectrum at $E = 3$ meV in the (HHL) plane. Calculated spin wave excitation spectra along the (d) $(-1-1L)$ (e) $(HH-1)$ directions. (f) Calculated constant-energy slice at $E = 3$ meV in the (HHL) plane. Measurements and calculations are further described in the text.

directions as shown in Figs. 3(a) and 3(b), respectively. The periodicity of the FM spectrum can clearly be seen in the constant-energy slice in the (HHL) plane at an energy transfer of 3 meV as shown in Fig. 3(c). Along both the (001) and (110) directions, the energy of the spin wave mode increases smoothly to ∼5.7 meV at the zone boundary, which is consistent with the bandwidth observed in the powder sample measurement.

To understand the spin excitations in GaV_4S_8, we develop an effective Hamiltonian based on molecular V_4 spins. Recently Dally *et al.* have argued that the spin distribution is uniform over the V_4 tetrahedra [33]. Therefore, for the description of the spin wave dispersion in GaV_4S_8, the breathing pyrochlore lattice formed by the V ions can be effectively treated as a face-centered-cubic (fcc) lattice of the V_4 molecular spins. A similar approach has been used to understand the spin-spin interactions in the Cr-breathing pyroclore materials [36–38]. Unlike the aforementioned Cr-based materials where intracluster interactions are evident, the uniform spin distribution over the V_4 tetrahedra only modulates the intensities through a magnetic form factor $\int d\boldsymbol{r} \exp(-i\boldsymbol{k}\boldsymbol{r})\rho(\boldsymbol{r})$, where $\rho(\boldsymbol{r})$ describes a ferromagnetic spin density that is equally distributed over the 4 V sites, and $\boldsymbol{k}$ is the wave-vector transfer. It should be noted that a recent neutron diffraction experiment on GaV_4S_8 proposed the spins within the V_4 tetrahedra may be tilted by an angle of $39(8)^\circ$ [39]. Such an uncertainty in spin alignment may modify the exact form of the V_4 form factor but will not qualitatively change our effective model as long as the major spin components are ferromagnetic. The coupling strengths between the V_4 spins can then be parametrized by comparing the experimental data to the dynamical spin structure factor on a fcc lattice. Using the linear spin wave theory implemented in the SPINW software package [40], we consider an effective model with nearest-neighbor (NN) exchange and DM interactions:

$$H = \sum_{\langle ij \rangle} J\boldsymbol{S}_i \cdot \boldsymbol{S}_j + \sum_{\langle ij \rangle} \boldsymbol{D} \cdot (\boldsymbol{S}_i \times \boldsymbol{S}_j), \tag{1}$$

where $\langle ij \rangle$ denotes the NN bonds with spins $\boldsymbol{S}_i$ and $\boldsymbol{S}_j$ located at the centers of the V_4 tetrahedra. The spin magnitude is assumed to be $S = 1/2$ per V_4 tetrahedra, which is consistent with the ordered moment of $\sim 0.25\mu_B$ per V ion [33]. The direction of the DM vector is fixed based on the fcc lattice symmetry. According to the cycloidal pitch and the mean-field analysis of magnetization measurements reported in Ref. [10], we fixed the DM interaction to the reported value of $D = 0.13$ meV. To fit the data, we extracted 26 different energy and momentum values from the experimentally observed spin waves along the high symmetry directions (110) and (001). A particle swarm oscillation (pso) fitting method implemented in the SPINW software package is used to fit the data. The spin wave modes within the energy bin size are binned together and considered as one mode in the fit. The fit to the two-dimensional (2D) dispersion data is carried out multiple times with more than 50 fitting cycles at each

time. The goodness of fit (or R value) of all those fits is around 2.7. Based on the value of the fitting parameter after all those runs, the value of exchange interaction J and its uncertainty is optimized as $-0.72(3)$ meV. As already noted, the DM interaction is fixed based on the cycloidal pitch and the mean field analysis of magnetization measurements reported in Ref. [10]. The ratio of D and J in GaV_4S_8 is around 0.18 which is comparable to many other skyrmion-host materials. For example, $D/J \sim 0.18$ stabilizes the skyrmion state in MnSi [41,42], whereas the nearest neighbor D/J value of 0.39 in the skyrmion-host bulk material Cu_2OSeO_3 [43] is larger than its value for GaV_4S_8. In the skyrmion ground state of a series of $Mn_{1-x}Fe_xGe$ ($0 < x < 1$) compounds [44], the value of D/J varies in the range 0.02–0.6 depending on the value of x.

The simulated powder average signal is presented in Figs. 2(c) and 2(d). A model obtained by accounting the form factor of V_4 tetrahedra, Fig. 2(d), reproduces the measured powder spin spectra with better reliability than a model with the form factor of single V^{3+} ion, Fig. 2(c), providing further support for the molecular picture for the V_4 tetrahedra. The exchange parameters reproduce spin-wave-like powder average excitation with zone center $|Q| = 0$. The calculated energy at each $|Q|$ overlaps with the experimentally measured excitation energy. As the form factor of V_4 tetrahedra changes significantly, our model indicates that the intensity of excitation spectrum decreases rapidly with the increase in the value of $|Q|$, consistent with the experimental observation. The simulated spin wave spectra, including all domain contributions, for single crystal measurements are shown in the lower panels of Fig. 3. The energy scale and the features of the calculated excitation spectrum are in accord with the experimental data.

Including further neighbor interactions does not result in a discernible increase in the quality of the fit with the present data set. Additionally, we note that the observed ferromagnetic ground state originates in part due to anisotropy which stems from the rhombohedral structural distortion at 44 K. Such anisotropic terms are to too small to be extracted from the data and analysis presented here.

Figures 4(a) and 4(b) present the scattering intensity at fixed energy transfers as a function of L along the $(-1\ -1\ L)$ and H along the $(H\ H\ -1)$ directions. Near the zone boundary, the line cuts shows broader peak width along the $(H\ H\ -1)$ direction compared to the $(-1\ -1\ L)$ direction. The calculated constant energy line cuts at the corresponding energies are overplotted to the data. The calculated line cuts successfully capture the peak position and broadness present in the data. The deviation between the model and the data near 5.5 meV is likely due to larger background scattering in this region of the spectrum.

We now compare the value of exchange coupling determined here with the value determined through other approaches [10,45]. Assuming the rhombohedral structure, Zhang *et al.* [45] calculated the NN (interplane) exchange coupling, using first-principles calculations and symmetry analysis. They found values in the range $[-0.16, -1.68]$ meV depending on the value of the effective Coulomb potential. They reported that a ratio D/J of $\sim$0.16 stabilizes the noncollinear spin structures in GaV_4S_8, which is consistent with our model. The scenario of different coupling

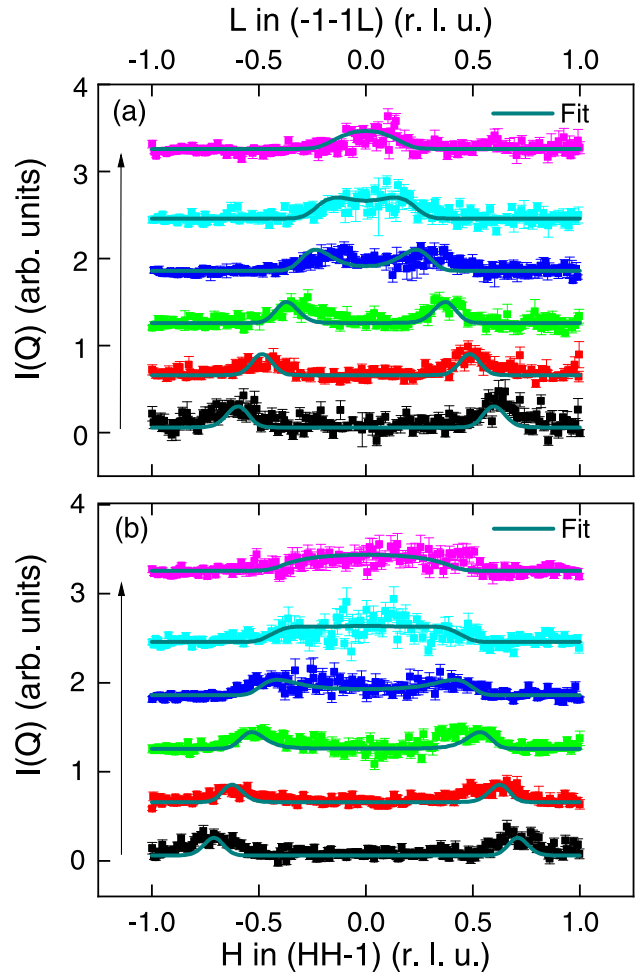

FIG. 4. Experimental (data points) and calculated (solid lines) constant-energy cuts at $E = 2$ meV (black squares), 3 meV (red squares), 4 meV (green squares), 5 meV (blue squares), 5.5 meV (cyan squares), and 6 meV (magenta squares) at 1.7 K (a) along the $(-1\ -\ 1L)$ direction and (b) along the $(HH\ -\ 1)$ direction. Error bars represent one standard deviation. The data at 3, 4, 5, 5.5, and 6 meV are shifted by 0.6, 1.2, 1.8, 2.4, and 3.2 along the y axis, respectively. The upward arrow in (a) and (b) indicates the direction of increasing energy transfer.

strengths due to the rhombohedral distortion is also discussed in Ref. [45]. Mean-field analysis of magnetization measurements in Ref. [10] showed the NN exchange interaction along the easy axis ~ -0.38 meV and an extremely weak magnetic anisotropy with a ratio of exchange couplings parallel and perpendicular to the easy axis $\sim$1.08. The single magnon mode observed in our MACS experiment suggests that the couplings strengths among the V_4 tetrahedra are close to uniform even in the rhombohedral phase. As noted previously, the experimental resolution of our measurements is not sufficient to distinguish small anisotropy terms; our value of exchange coupling J is fairly consistent with the value reported through other approaches.

IV. CONCLUSIONS

We have successfully grown single crystals of GaV_4S_8 of sufficient size to study the spin dynamics using INS. Our INS

experiments reveal well-defined spin wave excitations with a bandwidth of ∼6 meV, and an effective fcc lattice model of molecular V_4 spins reproduces the INS spectra. In addition to the ferromagnetic couplings of $J = -0.72(3)$ meV between neighboring V_4 spins, strong DM interactions with a magnitude of $D \sim 0.13$ meV are also confirmed. Our work clarifies the spin couplings in GaV_4S_8 and will facilitate the further understanding of its rich phase diagram.

ACKNOWLEDGMENTS

We thank C. Batista for useful discussions. This work was supported by the U.S. Department of Energy, Office of Science, Basic Energy Sciences, Materials Sciences and Engineering Division. G.P. acknowledges partial support from the Gordon and Betty Moore Foundations EPiQS Initiative Grant No. GBMF4416. G.P. also acknowledges support from UC Santa Barbara Quantum foundry through NSF DMR-1906325. H.S.A. acknowledges support from the Gordon and Betty Moore Foundation's EPiQS Initiative Grant No. GBMF9069. This research used resources at the Spallation Neutron Source and the High Flux Isotope Reactor, a Department of Energy (DOE) Office of Science User Facility operated by Oak Ridge National Laboratory (ORNL). Access to MACS was provided by the Center for High Resolution Neutron Scattering, a partnership between the National Institute of Standards and Technology and the National Science Foundation under Agreement No. DMR-1508249. This manuscript has been authored by UTBattelle, LLC under Contract No. DE-AC05-00OR22725 with the U.S. Department of Energy. The United States Government retains and the publisher, by accepting the article for publication, acknowledges that the United States Government retains a nonexclusive, paid-up, irrevocable, world-wide license to publish or reproduce the published form of this manuscript, or allow others to do so, for United States Government purposes. The Department of Energy will provide public access to these results of federally sponsored research in accordance with the DOE Public Access Plan [46].

[1] N. Nagaosa and Y. Tokura, Topological properties and dynamics of magnetic skyrmions, Nat. Nano. **8**, 899 (2013).

[2] G. Finocchio, F. Büttner, R. Tomasello, M. Carpentieri, and M. Kläui, Magnetic skyrmions: From fundamental to applications, J. Phys. D: Appl. Phys. **49**, 423001 (2016).

[3] A. Fert, N. Reyren, and V. Cros, Magnetic skyrmions: Advances in physics and potential applications, Nat. Rev. Mater. **2**, 17031 (2017).

[4] C. Back, V. Cros, H. Ebert, K. Everschor-Sitte, A. Fert, M. Garst, T. Ma, S. Mankovsky, T. L. Monchesky, M. Mostovoy, N. Nagaosa, S. S. P. Parkin, C. Pfleiderer, N. Reyren, A. Rosch, Y. Taguchi, Y. Tokura, K. von Bergmann, and J. Zang, The 2020 skyrmionics roadmap, J. Phys. D: Appl. Phys. **53**, 363001 (2020).

[5] X. Zhang, Y. Zhou, K. M. Song, T.-E. Park, J. Xia, M. Ezawa, X. Liu, W. Zhao, G. Zhao, and S. Woo, Skyrmion-electronics: Writing, deleting, reading and processing magnetic skyrmions toward spintronic applications, J. Phys.: Condens. Matter **32**, 143001 (2020).

[6] S. Mühlbauer, B. Binz, F. Jonietz, C. Pfleiderer, A. Rosch, A. Neubauer, R. Georgii, and P. Böni, Skyrmion lattice in a chiral magnet, Science **323**, 915 (2009).

[7] A. K. Nayak, V. Kumar, T. Ma, P. Werner, E. Pippel, R. Sahoo, F. Damay, U. K. Rößler, C. Felser, and S. S. P. Parkin, Magnetic antiskyrmions above room temperature in tetragonal Heusler materials, Nature (London) **548**, 561 (2017).

[8] X. Z. Yu, W. Koshibae, Y. Tokunaga, K. Shibata, Y. Taguchi, N. Nagaosa, and Y. Tokura, Transformation between meron and skyrmion topological spin textures in a chiral magnet, Nature (London) **564**, 95 (2018).

[9] S. Gao, H. D. Rosales, F. A. Gómez Albarracín, V. Tsurkan, G. Kaur, T. Fennell, P. Steffens, M. Boehm, P. Čermák, A. Schneidewind, E. Ressouche, D. C. Cabra, C. Rüegg, and O. Zaharko, Fractional antiferromagnetic skyrmion lattice induced by anisotropic couplings, Nature (London) **586**, 37 (2020).

[10] I. Kézsmárki, S. Bordács, P. Milde, E. Neuber, L. Eng, J. White, H. Rønnow, C. Dewhurst, M. Mochizuki, K. Yanai, H. Nakamura, D. Ehlers, V. Tsurkan, and A. Loidl, Néel-type skyrmion lattice with confined orientation in the polar magnetic semiconductor GaV_4S_8, Nat. Mater. **14**, 1116 (2015).

[11] E. Ruff, S. Widmann, P. Lunkenheimer, V. Tsurkan, S. Bordács, I. Kézsmárki, and A. Loidl, Multiferroicity and skyrmions carrying electric polarization in GaV_4S_8, Sci. Adv. **1**, e1500916 (2015).

[12] S. Widmann, E. Ruff, A. Günther, H.-A. K. von Nidda, P. Lunkenheimer, V. Tsurkan, S. Bordács, I. Kézsmárki, and A. Loidl, On the multiferroic skyrmion-host GaV_4S_8, Philos. Mag. **97**, 3428 (2017).

[13] T. Kurumaji, T. Nakajima, V. Ukleev, A. Feoktystov, T.-h. Arima, K. Kakurai, and Y. Tokura, Néel-Type Skyrmion Lattice in the Tetragonal Polar Magnet $VoSe_2O_5$, Phys. Rev. Lett. **119**, 237201 (2017).

[14] J. S. White, A. Butykai, R. Cubitt, D. Honecker, C. D. Dewhurst, L. F. Kiss, V. Tsurkan, and S. Bordács, Direct evidence for cycloidal modulations in the thermal-fluctuation-stabilized spin spiral and skyrmion states of GaV_4S_8, Phys. Rev. B **97**, 020401(R) (2018).

[15] E. M. Clements, R. Das, G. Pokharel, M. H. Phan, A. D. Christianson, D. Mandrus, J. C. Prestigiacomo, M. S. Osofsky, and H. Srikanth, Robust cycloid crossover driven by anisotropy in the skyrmion host GaV_4S_8, Phys. Rev. B **101**, 094425 (2020).

[16] S. Woo, K. Litzius, B. Krüger, M.-Y. Im, L. Caretta, K. Richter, M. Mann, A. Krone, R. M. Reeve, M. Weigand, P. Agrawal, I. Lemesh, M.-A. Mawass, P. Fischer, M. Kläui, and G. S. D. Beach, Observation of room-temperature magnetic skyrmions and their current-driven dynamics in ultrathin metallic ferromagnets, Nat. Mater. **15**, 501 (2016).

[17] S. Woo, K. M. Song, X. Zhang, Y. Zhou, M. Ezawa, X. Liu, S. Finizio, J. Raabe, N. J. Lee, S.-I. Kim, S.-Y. Park, Y. Kim, J.-Y. Kim, D. Lee, O. Lee, J. W. Choi, B.-C. Min, H. C. Koo, and J. Chang, Current-driven dynamics and inhibition of the skyrmion Hall effect of ferrimagnetic skyrmions in GdFeCo films, Nat. Commun. **9**, 959 (2018).

[18] Y. Wu, S. Zhang, J. Zhang, W. Wang, Y. L. Zhu, J. Hu, G. Yin, K. Wong, C. Fang, C. Wan, X. Han, Q. Shao, T. Taniguchi, K. Watanabe, J. Zang, Z. Mao, X. Zhang, and K. L. Wang, Néel-type skyrmion in WTe_2/Fe_3GeTe_2 van der Waals heterostructure, Nat. Commun. **11**, 3860 (2020).

[19] K. Xu and H. J. Xiang, Unusual ferroelectricity induced by the jahn-teller effect: A case study on lacunar spinel compounds, Phys. Rev. B **92**, 121112(R) (2015).

[20] M. M. Abd-Elmeguid, B. Ni, D. I. Khomskii, R. Pocha, D. Johrendt, X. Wang, and K. Syassen, Transition from Mott Insulator to Superconductor in $GaNb_4Se_8$ and $GaTa_4Se_8$ Under High Pressure, Phys. Rev. Lett. **93**, 126403 (2004).

[21] Y. Fujima, N. Abe, Y. Tokunaga, and T. Arima, Thermodynamically stable skyrmion lattice at low temperatures in a bulk crystal of lacunar spinel GaV_4Se_8, Phys. Rev. B **95**, 180410(R) (2017).

[22] E. Ruff, A. Butykai, K. Geirhos, S. Widmann, V. Tsurkan, E. Stefanet, I. Kézsmárki, A. Loidl, and P. Lunkenheimer, Polar and magnetic order in GaV_4Se_8, Phys. Rev. B **96**, 165119 (2017).

[23] E. Dorolti, L. Cario, B. Corraze, E. Janod, C. Vaju, H.-J. Koo, E. Kan, and M.-H. Whangbo, Half-metallic ferromagnetism and large negative magnetoresistance in the new lacunar spinel $GaTi_3VS_8$, J. Am. Chem. Soc. **132**, 5704 (2010).

[24] V. Ta Phuoc, C. Vaju, B. Corraze, R. Sopracase, A. Perucchi, C. Marini, P. Postorino, M. Chligui, S. Lupi, E. Janod, and L. Cario, Optical Conductivity Measurements of $GaTa_4Se_8$ Under High Pressure: Evidence of a Bandwidth-Controlled Insulator-to-Metal Mott Transition, Phys. Rev. Lett. **110**, 037401 (2013).

[25] P. Stoliar, L. Cario, E. Janod, B. Corraze, C. Guillot-Deudon, S. Salmon-Bourmand, V. Guiot, J. Tranchant, and M. Rozenberg, Universal electric-field-driven resistive transition in narrow-gap mott insulators, Adv. Mater. **25**, 3222 (2013).

[26] K. Singh, C. Simon, E. Cannuccia, M.-B. Lepetit, B. Corraze, E. Janod, and L. Cario, Orbital-Ordering-Driven Multiferroicity and Magnetoelectric Coupling in GaV_4S_8, Phys. Rev. Lett. **113**, 137602 (2014).

[27] K. Geirhos, S. Krohns, H. Nakamura, T. Waki, Y. Tabata, I. Kézsmárki, and P. Lunkenheimer, Orbital-order driven ferroelectricity and dipolar relaxation dynamics in multiferroic $GaMo_4S_8$, Phys. Rev. B **98**, 224306 (2018).

[28] Heung-Sik Kim, Jino Im, Myung Joon Han, and Hosub Jin, Spin-orbital entangled molecular jeff states in lacunar spinel compounds, Nat. Commun. **5**, 3988 (2014).

[29] H.-M. Zhang, J. Chen, P. Barone, K. Yamauchi, S. Dong, and S. Picozzi, Possible emergence of a skyrmion phase in ferroelectric $GaMo_4S_8$, Phys. Rev. B **99**, 214427 (2019).

[30] M. T. Warren, G. Pokharel, A. D. Christianson, D. Mandrus, and R. Valdés Aguilar, Terahertz dielectric analysis and spin-phonon coupling in multiferroic GeV_4S_8, Phys. Rev. B **96**, 054432 (2017).

[31] S. Reschke, F. Meggle, F. Mayr, V. Tsurkan, L. Prodan, H. Nakamura, J. Deisenhofer, C. A. Kuntscher, and I. Kézsmárki, Lattice dynamics and electronic excitations in a large family of lacunar spinels with a breathing pyrochlore lattice structure, Phys. Rev. B **101**, 075118 (2020).

[32] H. Müller, W. Kockelmann, and D. Johrendt, The magnetic structure and electronic ground states of Mott insulators GeV_4S_8 and GaV_4S_8, Chem. Mater. **18**, 2174 (2006).

[33] R. L. Dally, W. D. Ratcliff, L. Zhang, H.-S. Kim, M. Bleuel, J. W. Kim, K. Haule, D. Vanderbilt, S.-W. Cheong, and J. W. Lynn, Magnetic phase transitions and spin density distribution in the molecular multiferroic system GaV_4S_8, Phys. Rev. B **102**, 014410 (2020).

[34] G. E. Granroth, A. I. Kolesnikov, T. E. Sherline, J. P. Clancy, K. A. Ross, J. P. C. Ruff, B. D. Gaulin, and S. E. Nagler, SEQUOIA: A newly operating chopper spectrometer at the SNS, J. Phys.: Condens. Matter **251**, 012058 (2010).

[35] J. A. Rodriguez, D. M. Adler, P. C. Brand, C. Broholm, J. C. Cook, C. Brocker, R. Hammond, Z. Huang, P. Hundertmark, J. W. Lynn, N. C. Maliszewskyj, J. Moyer, J. Orndorff, D. Pierce, T. D. Pike, G. Scharfstein, S. A. Smee, and R. Vilaseca, MACS—a new high intensity cold neutron spectrometer at NIST, Meas. Sci. Technol. **19**, 034023 (2008).

[36] P. Ghosh, Y. Iqbal, T. Müller, R. T. Ponnaganti, R. Thomale, R. Narayanan, J. Reuther, M. J. P. Gingras, and H. O. Jeschke, Breathing chromium spinels: A showcase for a variety of pyrochlore heisenberg hamiltonians, npj Quantum Mater. **4**, 63 (2019).

[37] G. Pokharel, H. S. Arachchige, T. J. Williams, A. F. May, R. S. Fishman, G. Sala, S. Calder, G. Ehlers, D. S. Parker, T. Hong, A. Wildes, D. Mandrus, J. A. M. Paddison, and A. D. Christianson, Cluster Frustration in the Breathing Pyrochlore Magnet $LiGaCr_4S_8$, Phys. Rev. Lett. **125**, 167201 (2020).

[38] S. Gao, A. F. May, M.-H. Du, J. A. M. Paddison, H. S. Arachchige, G. Pokharel, C. de la Cruz, Q. Zhang, G. Ehlers, D. S. Parker, D. G. Mandrus, M. B. Stone, and A. D. Christianson, Hierarchical excitations from correlated spin tetrahedra on the breathing pyrochlore lattice, Phys. Rev. B **103**, 214418 (2021).

[39] S. J. R. Holt, C. Ritter, M. R. Lees, and G. Balakrishnan, Investigation of the magnetic ground state of GaV4s8 using powder neutron diffraction, J. Phys.: Condens. Matter **33**, 255802 (2021).

[40] S. Toth and B. Lake, Linear spin wave theory for single-q incommensurate magnetic structures, J. Phys.: Condens. Matter **27**, 166002 (2015).

[41] J. Iwasaki, M. Mochizuki, and N. Nagaosa, Universal current-velocity relation of skyrmion motion in chiral magnets, Nat. Commun. **4**, 1463 (2013).

[42] K. V. Shanavas and S. Satpathy, Electronic structure and the origin of the Dzyaloshinskii-Moriya interaction in MnSi, Phys. Rev. B **93**, 195101 (2016).

[43] J. H. Yang, Z. L. Li, X. Z. Lu, M.-H. Whangbo, S.-H. Wei, X. G. Gong, and H. J. Xiang, Strong Dzyaloshinskii-Moriya Interaction and Origin of Ferroelectricity in Cu_2OSeO_3, Phys. Rev. Lett. **109**, 107203 (2012).

[44] K. Shibata, X. Z. Yu, T. Hara, D. Morikawa, N. Kanazawa, K. Kimoto, S. Ishiwata, Y. Matsui, and Y. Tokura, Towards control of the size and helicity of skyrmions in helimagnetic alloys by spin–orbit coupling, Nat. Nanotechnol. **8**, 723 (2013).

[45] J. T. Zhang, J. L. Wang, X. Q. Yang, W. S. Xia, X. M. Lu, and J. S. Zhu, Magnetic properties and spin-driven ferroelectricity in multiferroic skyrmion host GaV_4S_8, Phys. Rev. B **95**, 085136 (2017).

[46] http://energy.gov/downloads/doe-public-access-plan.